PELLUCID INTERNATIONAL JOURNAL OF SCIENCE AND TECHNOLOGY (PIJSAT)
(PIJSAT), Issue 1, Vol.1. August 2025

https://pellucidjournal.com/pijsat/index

Exploring the Influence of Cycles Variation in SILAR Synthesized Manganese Oxide Thin Film

[1*]Akwolu, R.A., [1]Agbogu, A. N.C., [2]Alor, K. P. [1]Ayogu, C. O., and [1]Asogwa P.U.

[1]Department of Physics and Astronomy, University of Nigeria, Nsukka.

[2]Department of physics and industrial physics, Nnamdi Azikiwe University Awka

[1]rita.akwolu@unn.edu.ng, [1]ada.agbogu@unn.edu.ng [2]kp.alor@ unizik.edu.ng, [1]Christan.ayogu@gmail.com*
[1]paul.asogwa@unn.edu.ng, corresponding author: kp.alor@ unizik.edu.ng 08062152391

Abstract

Manganese oxide (MnO_2) thin films were synthesized on microscopic glass slide substrates using the successive ionic layer adsorption and reaction (SILAR) method. The deposition cycles (40, 50, 60, and 70) were varied to study their effect on structural and optical properties. X-ray diffraction (XRD) analysis revealed minimal variation among the films, confirming their amorphous nature, which is advantageous for pseudo capacitance applications. Scanning electron microscopy (SEM) showed Mn_3O_4 formation with nanoporous, mesh-like structures, which can enhance electrochemical performance. The direct band gap energies were calculated as approximately 1.9 eV (60 cycles), 2.0 eV (70 cycles), 2.2 eV (50 cycles), and 2.4 eV (40 cycles), indicating tunable optical properties. Fourier-transform infrared (FTIR) spectra for 40 cycles displayed absorption bands at 540, 720, and 1108 cm^{-1}, corresponding to hydroxyl (O-H), sulfate oxide (S-O), and metallic oxide (M-O) bonds. At 60 cycles, stronger and narrower peaks at 480, 520, and 600 cm^{-1} were observed, suggesting enhanced pseudocapacitive properties. The narrowing of peaks with increasing cycles indicates a more ordered structure within the amorphous matrix. This study highlights the potential of pseudocapacitive amorphous oxides for high-energy-density applications. The ability to tune the structural and optical properties of Mn_3O_4 thin films by varying deposition cycles presents significant advantages for energy storage devices. These findings underscore the importance of controlled synthesis in optimizing material performance for electrochemical applications.

Keyword: Manganese Oxide, SILAR, Optical, XRD, and FTIR

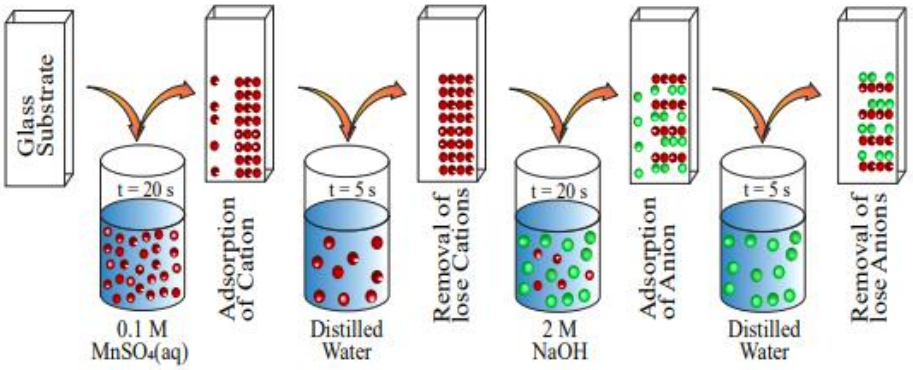

Graphical Abstracts of Manganese Oxide thin film using SILAR method

1.0 Introduction

The onset of the twenty-first century has marked a significant surge in global civilization and development, particularly in the aftermath of the world wars. This rapid advancement has necessitated an acute increase in energy requirements to support both domestic and industrial activities. Historically, a substantial portion of this energy has been sourced from fossil fuels, including crude oil, natural gas, coal, and wood. These fossil fuels are derived from the remains of organic matter, such as plants and animals that existed millions of years ago, having been transformed by geological processes (Smil, 2017).

In 2020, fossil fuels accounted for approximately 83% of total global energy consumption, underscoring the world's prevailing reliance on these non-renewable resources (BP, 2021). In response to the escalating energy demands and the urgent need to address climate change, various initiatives have been explored to identify alternative energy solutions. Nuclear power has gained traction as a viable option, allowing for a reduction in carbon emissions and presenting a pathway towards a more sustainable energy future (World Nuclear Association, 2021).

Solar energy has emerged as a particularly promising alternative within the renewable energy sector. Multiple innovative methodologies have been developed to harness solar power, categorized into three primary techniques: photochemical, photoelectrical, and photothermal conversion (Chow, 2010). The process of photosynthesis exemplifies photochemical conversion, facilitating the sustenance of life on Earth by enabling plants to convert sunlight into energy (Blankenship et al., 2011).

Photothermal systems also contribute significantly by capturing solar radiation for heating applications, such as water heating. Of particular importance is photoelectrical conversion, which directly transforms sunlight into electricity through photovoltaic (PV) cells. This technology is critical for the advancement of solar energy utilization, and extensive research efforts have been directed toward enhancing the efficiency and affordability of PV modules to meet a considerable share of global energy requirements (Green et al., 2015).

Nevertheless, the challenge of fulfilling a significant portion of the world's energy demand through solar photovoltaic means remains considerable, especially given the current dominance of fossil fuels. As a result, researchers are actively investigating thin-film technologies as a promising alternative for future advancements in solar energy production, potentially paving the way for a more sustainable energy landscape (Basore, 2018).

Manganese oxide (Mn_3O_4) is a material distinguished by its remarkable physical and chemical properties, positioning it as a pivotal component in a range of optoelectronic applications. It is extensively utilized as an electrode material in electrochemical capacitors, rechargeable batteries, catalysts, and magneto-electronic devices (Chakraborty et al., 2019). Furthermore, Mn_3O_4 is integral to the synthesis of magnetic oxide perovskite compounds, which exhibit a diverse array of electrical and magnetic characteristics, including functionalities such as metal-insulator transistors and colossal magneto-resistance (Zhang et al., 2018).

Various structural variants of Mn_3O_4 can be deposited employing a multitude of techniques. Noteworthy methods include successive ionic layer absorption and reaction (SILAR), chemical bath deposition, sol-gel processes, spin coating, electrodeposition, pulsed laser deposition, atomic layer deposition, and thermal evaporation. SILAR, in particular, is recognized for its cost-effectiveness and its capacity for low-temperature wet chemical solutions (Pathan & Lokhande, 2004). This method involves a series of consecutive reactions on the

substrate surface, with rinsing protocols implemented between each reaction stage. Such rinsing promotes heterogeneous reactions between the solid phase and solvated ions present in the solution.

The SILAR technique facilitates the layer-by-layer growth of thin films and is characterized by exceptional material utilization efficiency. Moreover, it offers precise control over the deposition process, including the engineering of film thickness. Additionally, SILAR enables large-scale deposition on various substrate types, thereby demonstrating significant versatility and effectiveness within the field of materials science (Lokhande et al., 2013).

2.1 Materials and Methods

Successive Ionic Layer Adsorption and Reaction represents a novel chemical approach for the deposition of thin films. In the synthesis of Mn_3O_4 films, a 0.1 M manganese (II) sulfate ($MnSO_4$) solution was utilized as the cationic precursor, while a 2.0 M NaOH solution served as the anionic precursor.

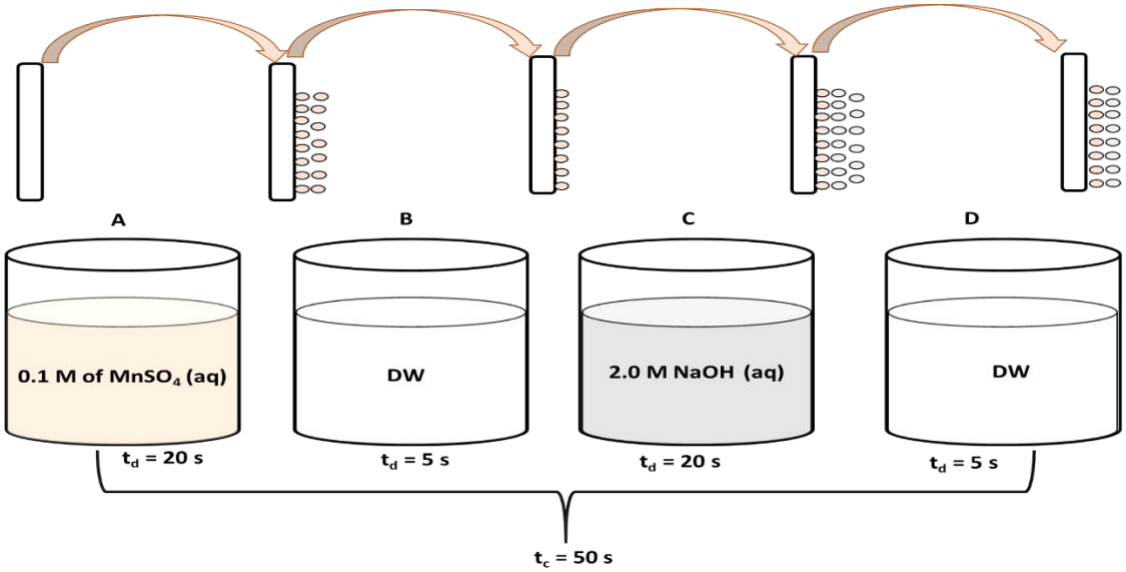

Figure 1: A Schematic diagram of the SILAR deposition technique

The experimental setup consisted of four sets of 50-milliliter beakers, designated A, B, C, and D. Beaker A contained a manganese sulfate solution, while beaker B was filled with distilled water. Beaker C held a sodium hydroxide solution, and Beaker D also contained distilled water. A thoroughly cleaned glass substrate, prepared by sequentially rinsing with acid, distilled water, and acetone, was immersed in the cationic precursor solution (Mn_3O_4) for 20 seconds to facilitate the adsorption of manganese ions onto the substrate surface. Following this, the substrate was rinsed in distilled water for 5 seconds to eliminate loosely bound Mn2+ ions. Subsequently, the substrate was immersed in the anionic precursor solution (NaOH) for an additional 20 seconds to form a layer of manganese oxide (Mn_3O_4). The substrate underwent another rinsing in deionized water for 5 seconds to remove any unbound ions, thereby completing one cycle of successive ionic layer adsorption and reaction (SILAR) for the synthesis of Mn_3O_4. The chemical reactions involved in the SILAR formation of manganese oxide using manganese sulfate and sodium hydroxide as precursors are as follows:

i. Adsorption of Manganese Ions onto Substrate:

$$Mn^{2+}_{(aq)} + 2OH^{-}_{(aq)} \rightarrow Mn(OH)_{2(s)}$$

ii. Oxidation of Manganese Hydroxide to Manganese Oxide:

$$Mn(OH)_{2(s)} + \frac{1}{2}O_2 \rightarrow MnO_{2(s)} + H_2O_{(l)}$$

iii. Formation of Manganese Oxide (Mn_3O_4):

$$MnO_{2(s)} + Mn^{2+}_{(aq)} + 2OH^{-}_{(aq)} \rightarrow Mn_3O_{4(s)} + 2H_2O$$

The experimental procedure was conducted at room temperature for a series of cycles: 40, 50, 60, and 70, yielding four samples characterized by varying thicknesses. The chemical compositions of the thin films produced in this study were determined through phase identification employing XRD with an MD-10 diffractometer, configured to operate at a voltage of 20 kV and a current of 20 mA. The morphology and dimensions of the synthesized particles were analyzed using a scanning electron microscope (SEM) model A-VPSEG3, which operated at an acceleration voltage of 20 kV and encompassed a magnification range from 1000x to 10000x. Furthermore, the optical properties of the deposited films were assessed for absorbance and transmittance at normal incidence utilizing a UV-visible spectrophotometer.

3.0 Results and Discussions

3.1 Optical properties of Mn_3O_4 films

The absorption spectra of the deposited Mn_3O_4 thin films were measured across a wavelength range of 400 to 1000 nm, depicted in Figure 2a. The results indicated a clear trend: absorbance decreases as wavelength increases. Notably, there was a high absorption rate at 400 nm, while absorbance values showed a significant decline within the visible spectrum, approaching near-infrared wavelengths where absorbance nearly vanishes. This trend reinforces the concept that absorbance is inversely related to the wavelength of electromagnetic radiation.

At 600 nm, absorbance values were recorded at 0.25, 0.42, 0.65, and 0.85 a.u. for deposition cycles of 40, 50, 70, and 60, respectively. A key observation was that the absorption edge shifted from 450 nm to 650 nm between the 40 and 60 cycles. This suggests that the film deposited at 60 cycles achieved the highest absorbance value, indicating it may represent the optimal deposition cycle. Beyond this point, however, the deposited layer appeared to wash out, likely due to challenges related to improper nucleation stemming from surface saturation and increased stress from thicker layers.

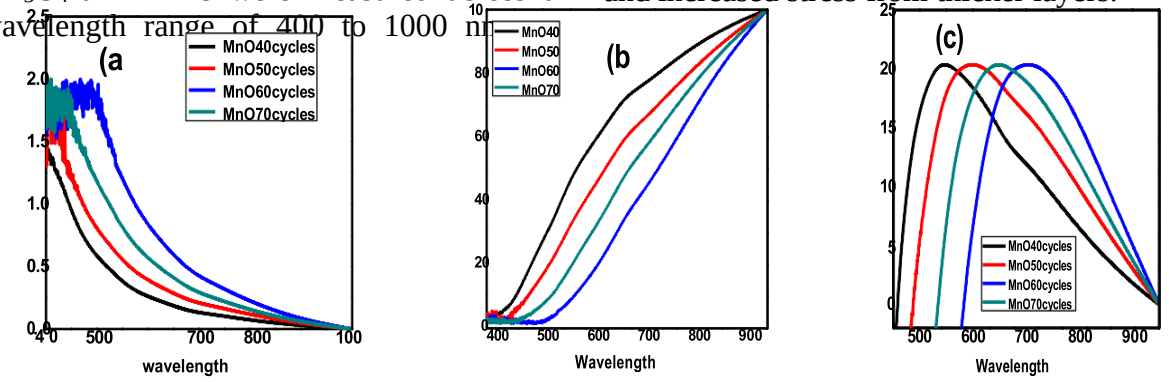

Figure2: Plot of absorbance (a), transmittance (b), and reflectance(c)

Figure 2b illustrates the transmittance of Mn_3O_4 thin films with respect to wavelength. The data showed that transmittance was quite low at 400–500 nm but increased significantly for wavelengths above 500 nm, demonstrating a clear advantage in higher transmittance. The film synthesized at 40 cycles displayed the highest transmittance, while the film at 60 cycles had the lowest within the visible spectrum. This suggests an important relationship: as the number of SILAR cycles increased, the films became thicker, resulting in reduced transparency. However, the enhanced transmittance in the visible spectrum highlights the potential for these films to be utilized in energy-saving or heat-protecting window applications. Furthermore, the higher transmittance in the near-infrared region suggests promising applications as solar collectors in batteries (Ezema et al., 2010).

The analysis of reflectance, as shown in Figure 2c, indicated that Mn3O4 thin films exhibited increasing reflectance with longer wavelengths in the visible range. The average reflectance was approximately 20% at wavelengths of 550 nm, 600 nm, 650 nm, and 700 nm, corresponding to deposition cycles of 40, 50, 70, and 60, respectively. This finding underlines the impact of varying deposition cycles on optical reflectance, which can be particularly beneficial in the development of integrated circuits. (Zhang et al., 2017)

Overall, these insights pave the way for further exploration of Mn_3O_4 films in various applications, enhancing our understanding of their optical properties and potential uses.

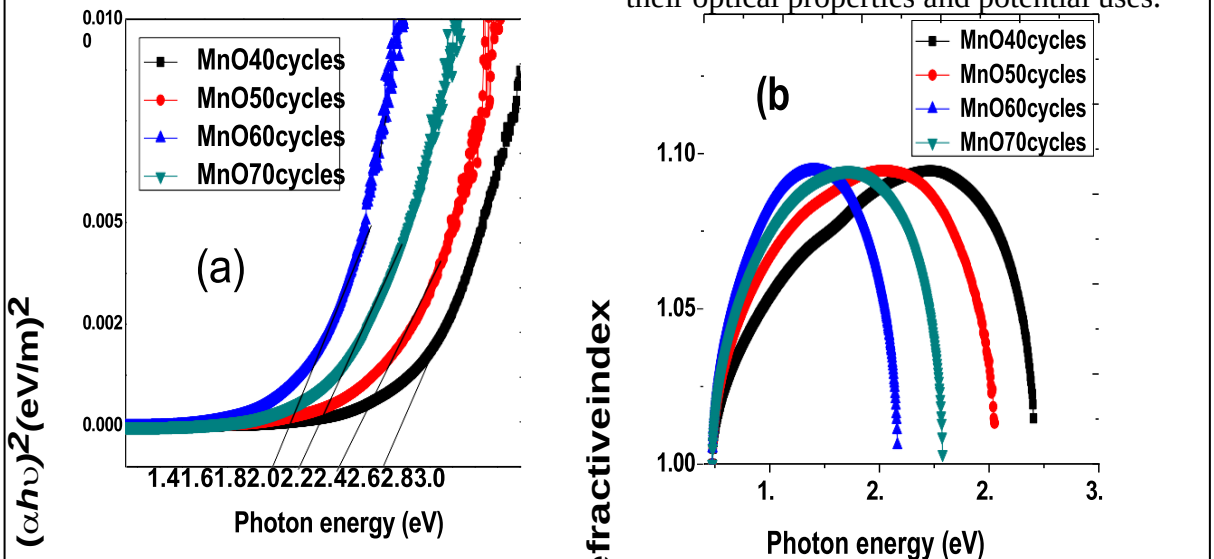

Figure 3: Plot of $(\alpha hv)^2$ (a) and Refractive index(b) of MnO

A plot of $(\alpha h\nu)^2$ versus photon energy for Mn_3O_4 films is illustrated in Figure 3a. The linear section of the curve where $(\alpha h\nu)^2 = 0$ allows us to determine the energy bandgap values (Eg), which are 1.9 eV, 2.0 eV, 2.2 eV, and 2.4 eV for films deposited at 60, 70, 50, and 40 cycles, respectively. This indicates that the number of deposition cycles has a significant impact on the energy bandgap of the synthesized Mn_3O_4 thin films. The energy bandgap values identified in this study are consistent with the range of 1.25 - 3.30 eV reported in earlier research (Ambreen et al., 2021; Fakharpour & Karimi, 2022; Ahmad et al., 2024;).

Figure 3b depicts the refractive index as a function of photon energy, revealing important observations about the Mn_3O_4 films. It was found that all deposited thin films display peak refractive index values at varying photon energies. Specifically, maximum refractive index values were recorded for films deposited at 60, 70, 50, and 40 cycles at photon energies of 1.75 eV, 2.0 eV, 2.15 eV, and 2.30 eV, respectively. The relatively low refractive index values (1.0 - 1.10) may result from successive total reflection or trapped photon energy at the grain boundaries (Taunk et al., 2015).
This also highlights that variations in the deposition cycle influence the refractive index values of the Mn_3O_4 thin films produced.

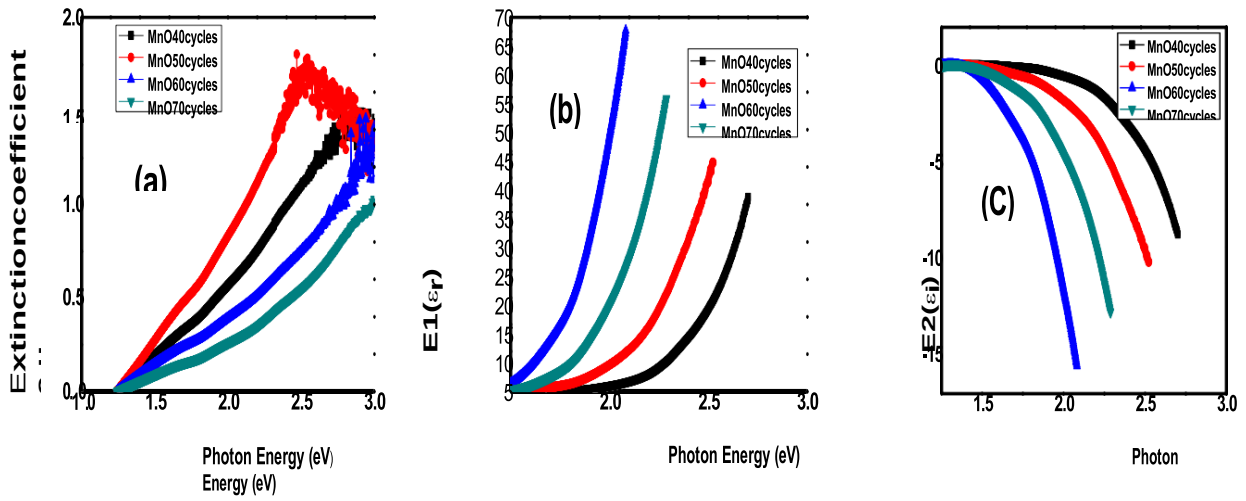

Figure4: A plot of extinction coefficient (a), Real dielectric constant (b), and imaginary dielectric constant (c) of Mn_3O_4 thin films

Figures 4a, 4b, and 4c provide a detailed examination of the optical properties of Mn_3O_4 thin films, highlighting how deposition cycles influence these characteristics. These findings align with and expand upon trends observed in recent studies.

Figure 4a illustrates the relationship between the extinction coefficient and photon energy. As photon energy increases, so does the extinction coefficient, indicating enhanced absorption. Notably, the film deposited at 50 cycles exhibits a higher extinction coefficient than that at 40 cycles, while the 70-cycle film shows a lower coefficient compared to the 60-cycle film. This non-linear behavior suggests that film thickness and morphology, which are influenced by deposition cycles, play a significant role in optical absorption. Such variations are consistent with the findings of

Ozkan et al. (2018), who observed that the number of deposition cycles affects the structural and optical properties of Mn_3O_4 thin films, including the extinction coefficient.

Figure 4b examines the real part of the dielectric constant (ε_1), showing an increase with photon energy. The highest dielectric constant is observed in the sample deposited at 60 cycles, while the 40- and 50-cycle films display lower values. The films are thinner and more transparent at lower deposition cycles, which could be advantageous for applications requiring low dielectric constants, such as antireflective coatings. This trend is supported by the work of Pandey et al. (2023), who reported that the dielectric properties of Mn_3O_4 films are influenced by the number of coating layers, affecting their suitability for various electronic applications.

Figure 4c depicts the variation of the imaginary part of the dielectric constant (ε_2) with photon energy. Unlike ε_1, ε_2 decreases as photon energy increases. The film deposited at 60 cycles exhibits the highest ε_2 values, suggesting that greater energy dissipation at lower energies is desirable for light-harvesting layers. This observation aligns with the conclusions of Ozkan et al. (2018), who noted that the number of deposition cycles affects the imaginary part of the dielectric constant in Mn_3O_4 thin films.

Together, these observations underscore how deposition cycles critically influence the optical behavior of Mn_3O_4 films. The data not only aligns with prior research but also reinforces the potential of Mn_3O_4 as a tunable material for next-generation optoelectronic and photovoltaic devices.

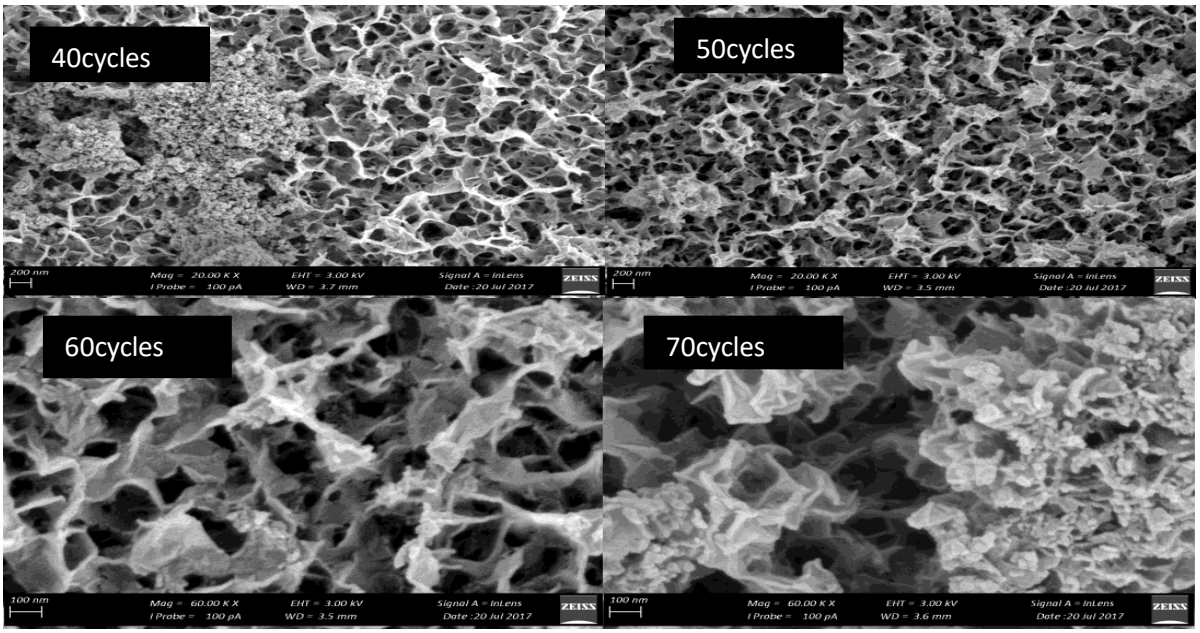

Figure 5: SEM images of Mn_3O_4deposited samples.

The surface morphology of manganese oxide thin films, illustrated in Figure 5, exhibits a compact structure with smooth, uniquely shaped grains that include nanoflakes and nanowires of various sizes. Observations at 50 and 60 cycles under high magnification (200 nm) reveal an interconnected arrangement of these grains, forming mesh-like structures. This arrangement of unintegrated grain shapes contributes to a highly porous array composed of nanoscale Mn_3O_4 particles. The

promising nanoporous characteristics of Mn_3O_4 suggest its potential as an effective electrode material for supercapacitors (Shaik et al., 2019).

3.2 XRD ANALYSIS

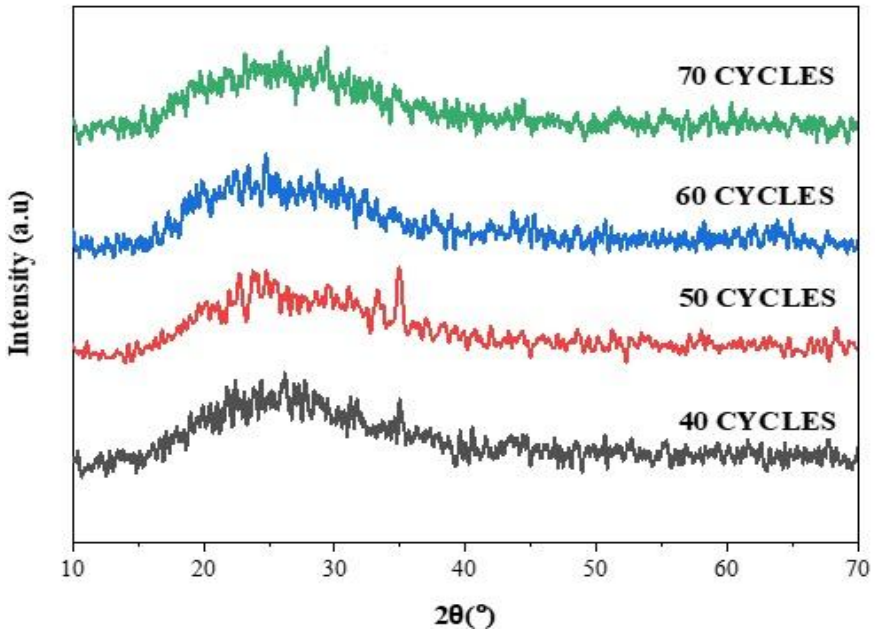

Figure 6: XRD pattern of Mn_3O_4 for40, 50, 60 and 70 cycles.

The X-ray diffraction (XRD) patterns of Mn_3O_4 thin films deposited on glass substrates for 40, 50, 60, and 70 cycles show no significant variation. The lack of distinct diffraction peaks in the films suggests that they consist of amorphous manganese oxide particles. Amorphous oxides with pseudocapacitive properties are considered promising materials for applications requiring

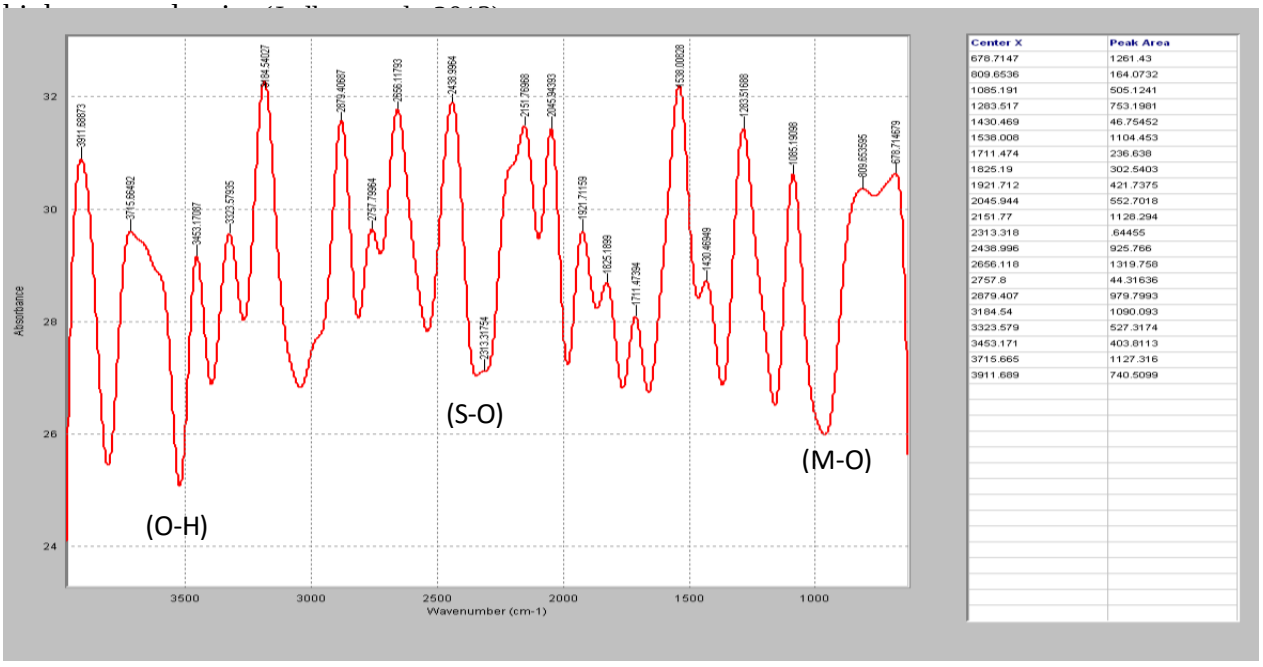

Figure 6: A plot of the FTIR of deposited Mn_3O_4 at 40 cycles

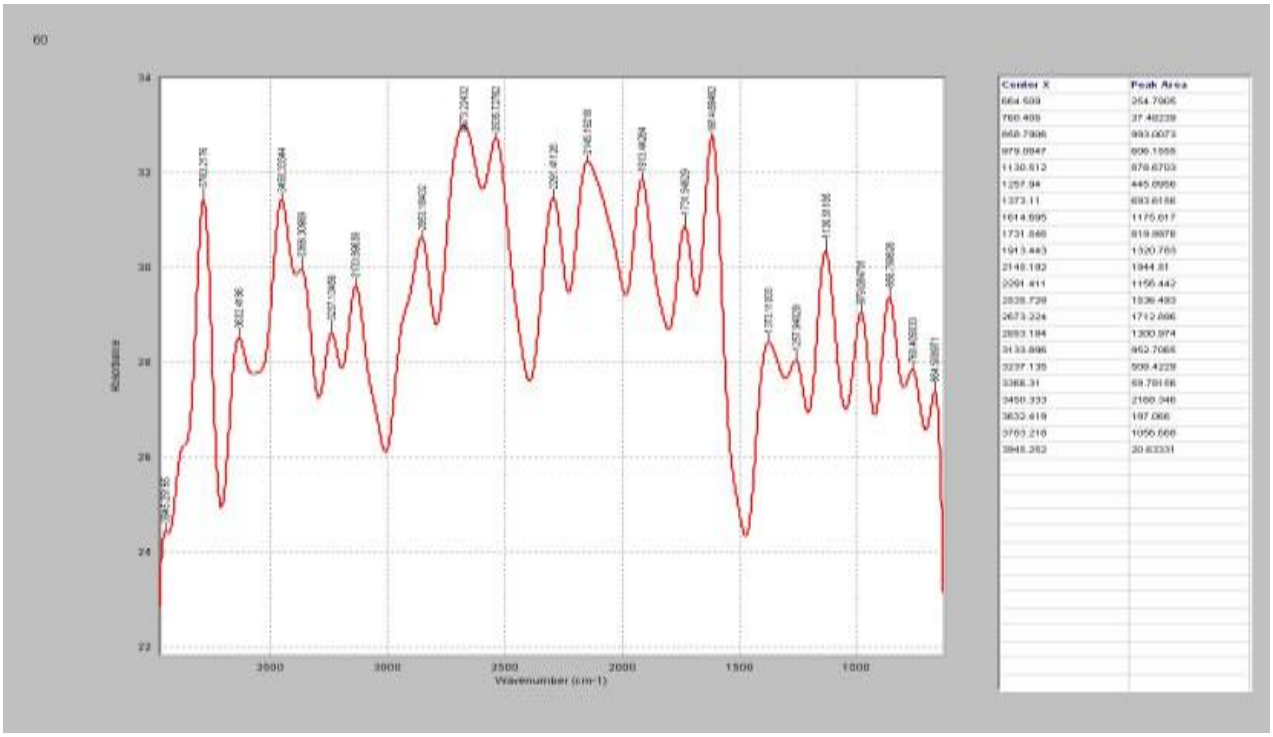

Figure 7: A plot of the FTIR of deposited Mn_3O_4 at 60 cycles

3.3 Fourier TransformInfra-Red (FTIR) Analysis

The Fourier Transform Infrared (FTIR) analysis presented in Figures 6 and 7 illustrates the transmission spectrum of Mn_3O_4 deposited at 40 and 60 cycles, recorded with radiation at a normal angle of incidence. Analyzing the spectrum is somewhat complex due to the presence of various functional groups, such as O-H and S-O groups. Additionally, many important features exhibit two peaks, which arise from in-phase and out-of-phase vibrational interactions among different chemical species. The fundamental vibration components occur at higher frequencies (Patro et al., 2023).

At 40 cycles, the spectrum displays three distinct bands corresponding to O-H (hydroxyl), S-O (sulfate oxide), and M-O (metallic oxide), with peak values at 540, 720, and 1108 cm^{-1} respectively. The strong band at 540 cm^{-1} is attributed to the Mn_3O_4 phase (Isber et al., 2009). At 60 deposition cycles, three distinct FTIR peaks appear at approximately 480 cm^{-1}, 520 cm^{-1}, and 600 cm^{-1}. These peaks are noticeably sharper and narrower compared to those seen at 40 cycles, suggesting an improvement in the crystal quality of the Mn_3O_4 thin films as the number of deposition cycles increase. Narrower peaks typically indicate reduced structural defects and better phase formation, which point to more ordered crystal growth.

These FTIR peaks correspond to the MnO stretching vibrations associated with the spinel structure of Mn_3O_4, particularly involving both tetrahedrally coordinated Mn^{2+} and octahedrally coordinated Mn^{3+} ions. The observed vibrational modes are in good agreement with previous studies on Mn_3O_4 materials, confirming the successful formation of the spinel phase. Specifically,

these results are consistent with findings by Parveen et al. (2022), who reported similar characteristic peaks in Mn_3O_4 structures with improved crystallinity at higher synthesis or deposition parameters.
This alignment with existing literature supports the conclusion that increasing the deposition cycles enhances structural ordering in Mn_3O_4 thin films, which is beneficial for their performance in electronic, catalytic, and sensing applications.

The strong peaks in the range of 480 to 600 cm^{-1} are associated with the vibrational modes of Mn_3O_4 (Gayathri et al., 2023).

Very weak bands corresponding to MnO_2 appeared around 720 cm^{-1} and higher at all deposition cycle variations, suggesting that this phase does not significantly grow under these deposition conditions. The FTIR results for the 40-cycle samples, supported by X-ray diffraction (XRD) data, confirm that most of the peaks correspond to Mn_3O_4, and the prominent peaks observed at 60 cycles are also associated with the Mn_3O_4 phase.

3.4 Conclusion

In conclusion, this study effectively demonstrates the synthesis of manganese oxide (MnO_2) thin films on glass substrates using the Successive Ionic Layer Adsorption and Reaction (SILAR) method. By varying the deposition cycles (40, 50, 60, and 70 cycles), we assessed their effects on the structural and optical properties of the films. The results indicate that, regardless of the number of cycles, the films remained amorphous, a characteristic that is beneficial for pseudocapacitive applications.

The Scanning Electron Microscopy (SEM) analysis revealed the formation of Mn_3O_4 alongside nano-porous, mesh-like structures. These features suggest potential improvements in the electrochemical performance of the films, making them promising candidates for energy storage technologies. Additionally, the variation in band gap energy across different deposition cycles provides a degree of tunability, allowing us to tailor the optical properties to meet specific application needs.

Notably, Fourier Transform Infrared (FTIR) analysis identified distinct vibrational modes, which imply improved structural order at higher deposition cycles, thereby enhancing the pseudocapacitive behavior.

Overall, this study highlights the potential of Mn_3O_4 thin films as viable materials for high-energy-density applications, particularly in the field of energy storage devices. The ability to modulate both the structural and optical characteristics of these films through variations in deposition cycles offers significant flexibility, paving the way for the development of more efficient and adaptable energy storage technologies.

Declaration of Conflict of Interest:

The authors were able to declare that there is no conflict of interest.

Acknowledgments:

The authors wish to acknowledge all the astute researchers at the Physics and Astronomy University of Nigeria, Nsukka, particularly Prof. F. Ezema and Prof. Mrs. A.N.C. Agbogu, whose concern, support, and prayers inspired this work.

References

Ahmad, M., Ahmad, M., Aziz, M. H., & Asif, M. (2024). Structural, morphological, mechanical, and electronic properties of nickel-substituted manganese oxide (NixMn1−xO, x = 0.0, 0.2, 0.4) for electronic applications. *Heliyon, 10*(5), e26708. https://doi.org/10.1016/j.heliyon.2024.e26708

Basore, P. A. (2018). Defining terms for photovoltaics. *Nature Energy, 3*(6), 438-440.

https://doi.org/10.1038/s41560-018-0197-0

Blankenship, R. E., Tiede, D. M., Barber, J., Brudvig, G. W., Fleming, G., Ghirardi, M., ... & Zinth, W. (2011). Comparing photosynthetic and photovoltaic efficiencies and recognizing the potential for improvement. *Science, 332*(6031), 805-809. https://doi.org/10.1126/science.1200165

BP. (2021). *Statistical review of world energy 2021*. BP Global. https://www.bp.com/en/global/corporate/energy-economics/statistical-review-of-world-energy.html

Chakraborty, D., Das, D., & Banerjee, S. (2019). Manganese oxide nanoparticles: Synthesis, properties, and applications. *Journal of Materials Science, 54*(12), 8975-9002. https://doi.org/10.1007/s10853-019-03411-7

Chow, T. T. (2010). A review on photovoltaic/thermal hybrid solar technology. *Applied Energy, 87*(2), 365-379. https://doi.org/10.1016/j.apenergy.2009.06.037

Ezema, F. I., Ezugwu, S. C., Osuji, R. U., Asogwa, P. U., Ezekoye, B. A., Ekwealor, A. B. C., & Ogbu, M. P. (2010). Role of thermal annealing on the optical and solid-state properties of chemically deposited cadmium sulfate nanocrystalline thin film grown on polymer matrix. *Journal of Non-Oxide Glasses, 1*, 45-50.

Fakharpour, M., & Karimi Tafti, M. H. (2022). The energy band gap of the manganese oxide pyramidal nanostructures. *Journal of Modern Optics, 69*(16), 911-916. https://doi.org/10.1080/09500340.2022.2095050

Gayathri, V., Amaladass, E. P., Sathyanarayana, A. T., Geetha Kumary, T., Pandian, R., Gupta, P., Rai, S. K., & Mani, A. (2023). Interfacial interaction driven enhancement in the colossal magnetoresistance property of ultra-thin heterostructure of Pr0.6Sr0.4MnO3 in proximity with Pr0.5Ca0.5MnO3. *Scientific Reports, 13*(1), 2315. https://doi.org/10.1038/s41598-023-28314-8

Green, M. A., Hishikawa, Y., Dunlop, E. D., Levi, D. H., Hohl-Ebinger, J., Yoshita, M., & Ho-Baillie, A. W. (2015). Solar cell efficiency tables (version 45). *Progress in Photovoltaics: Research and Applications, 23*(1), 1-9. https://doi.org/10.1002/pip.2573

Isber, S., Majdalani, E., Tabbal, M., Christidis, T., Zahraman, K., & Nsouli, B. (2009). Study of manganese oxide thin films grown by pulsed laser deposition. *Thin Solid Films, 517*, 1592–1595. https://doi.org/10.1016/j.tsf.2008.09.097

Jadhav, P. R., Shinde, V. V., Navathe, G. J., Karanjkar, M. M., & Patil, P. S. (2013). Manganese oxide thin films deposited by SILAR method for supercapacitor application. *AIP Conference Proceedings, 1536*, 679-680. https://doi.org/10.1063/1.4810409

Khan, S., Hussain, A., He, K., Liu, B., Imran, Z., Ambreen, J., Hassan, S., Ahmad, M., Batool, S. S., & Li, C. (2021). Tailoring the bandgap of Mn3O4 for visible light driven photocatalysis. *Journal of Environmental Management, 293*, 112854. https://doi.org/10.1016/j.jenvman.2021.112854

Lokhande, C. D., Dubal, D. P., & Joo, O. S. (2013). Metal oxide thin film-based supercapacitors. *Current Applied Physics, 13*(6), 391-414. https://doi.org/10.1016/j.cap.2013.02.002

Ozkan B., Onder S., Harun G., Erdal I., & Mustafa M.O., (2018) *Journal of Materials Science: Materials in Electronics*. "Effect of the number of cycles on the optical and structural properties of Mn_3O_4 nanostructures obtained by SILAR technique" and can be accessed via the DOI: 10.1007/s10854-018-9118-9

Pandey, V., Siddiqui, M. S., Munjal, S., & Ahmad, T. (2023). *Structural and Optical Properties of Spin-Coated Mn_3O_4 Thin Films of Different Coating Layers*. https://doi.org/10.48550/arXiv.2308.05728

Parveen, N., Ansari, S. A., Ansari, M. Z., & Ansari, M. O. (2022). Manganese oxide as an effective electrode material for energy storage: A review. *Environmental Chemistry Letters, 20*(1), 283-309. https://doi.org/10.1007/s10311-021-01316-6

Patro, A., Rajbhar, M. K., Chatterjee, S., Patra, A., Rout, C. S., & Dhal, S. (2023). Augmented electrochemical properties of manganese oxide nanorods on low energy nitrogen ion irradiation. *Journal of Alloys and Compounds, 960*, 170441. https://doi.org/10.1016/j.jallcom.2023.170441

Pathan, H. M., & Lokhande, C. D. (2004). Deposition of metal chalcogenide thin films by successive ionic layer adsorption and reaction (SILAR) method. *Bulletin of Materials Science, 27*(2), 85-111. https://doi.org/10.1007/BF02708491

Shaik, D. P. M., Pitcheri, R., Qiu, Y., & Hussain, O. M. (2019). Hydrothermally synthesized porous Mn3O4 nanoparticles with enhanced electrochemical performance for supercapacitors. *Ceramics International, 45*(2, Part A), 2226-2233. https://doi.org/10.1016/j.ceramint.2018.10.135

Smil, V. (2017). *Energy and civilization: A history.* MIT Press.

Taunk, P. B., Das, R., Bisen, D. P., Tamrakar, R. K., & Rathor, N. (2015). Synthesis and optical properties of chemical bath deposited ZnO thin film. *Karbala International Journal of Modern Science, 1*(3), 159-165. https://doi.org/10.1016/j.kijoms.2015.11.002

World Nuclear Association. (2021). *Nuclear power and the environment.* https://www.world-nuclear.org/information-library/current-and-future-generation/nuclear-power-and-the-environment.aspx

Zhang, C., Hao, F., Gao, G., Liu, X., Ma, C., Lin, Y., Yin, Y., & Li, X. (2017). Enhanced superconductivity in TiO epitaxial thin films. *npj Quantum Materials, 2*(1), 2. https://doi.org/10.1038/s41535-016-0006-3

Zhang, W., Zhang, M., & Wang, L. (2018). Magnetic perovskite oxides: Structure, properties, and applications. *Advanced Materials, 30*(30), 1706983. https://doi.org/10.1002/adma.201706983